Volume 267, Issues 1–2 1 March 2008 ISSN 0012-821X

ELSEVIER

EARTH & PLANETARY SCIENCE LETTERS

Available online at www.sciencedirect.com
ScienceDirect
Earth and Planetary Science Letters 267 (2008) 236–246
EPSL
www.elsevier.com/locate/epsl

U–Pb dating of fossil enamel from the Swartkrans Pleistocene hominid site, South Africa

Vincent Balter [a,*], Janne Blichert-Toft [b], José Braga [c], Philippe Telouk [b], Francis Thackeray [d], Francis Albarède [b]

[a] *UMR 5125 "PaléoEnvironnements et PaléobioSphère", CNRS, France; Université Lyon 1, Campus de la Doua, Bâtiment Géode, 69622 Villeurbanne Cedex, France*
[b] *UMR 5570 "Laboratoire de Sciences de la Terre", CNRS, France; Ecole Normale Supérieure de Lyon-Université Lyon 1, 46 Allée d'Italie, 69364 Lyon Cedex 7, France*
[c] *FRE 2960 "Laboratoire d'Anthropobiologie", CNRS, France; Université Toulouse 3, 39 Allées Jules Guesde, 31000 Toulouse, France*
[d] *Transvaal Museum, PO Box 413, Pretoria 0001, South Africa*

Received 13 June 2007; received in revised form 8 November 2007; accepted 22 November 2007
Available online 14 December 2007
Editor: H. Elderfield

Abstract

We demonstrate that young fossil enamel older than the range of the U-series (~300 ka) can be dated by the U–Pb methods using new models of U and Pb loss and uptake. Contrary to the current hypothesis of U uptake that only considers the adsorption/diffusion mechanism, we here develop a complete time-dependent model which takes gains and losses of the most critical nuclides (^{238}U, ^{234}U, and ^{230}Th) into account, both during chemical (dissolved U) and physical (Th and U α-recoil) processes. Lead is assumed to be a mixture between two components of common Pb and a radiogenic component; the proportions of these components are calculated from the Pb isotope abundances and U/Pb ratios. We apply this new U–Pb method to bovid enamel from the Swartkrans Cave (Gauteng Province, South Africa). This cave has yielded abundant early Pleistocene hominid remains attributed to *Paranthropus* and *Homo* as well as various associated archaeological vestiges. Biochronological comparisons with East Africa have provided age estimates ranging between 1.8 and 1.0 Ma, which, however, remain poorly constrained. After correction for initial ^{234}U disequilibrium and further ^{238}U loss, the U and Pb isotope data yield ages of 1.83±1.38, 1.36±0.29, and 0.83±0.21 Ma for the three stratigraphic units, Members 1, 2, and 3, respectively. We discuss the consequences of these radiometric results for hominid evolution in South Africa.

Keywords: geochronology; Plio–Pleistocene; U-series disequilibrium; U–Pb dating; teeth

1. Introduction

The caves of the Sterkfontein Valley in the Gauteng Province, South Africa, are among the richest hominid-bearing localities in Africa (Fig. 1). Swartkrans, which was discovered in 1948, is one of the most renowned of these caves because of its abundant early Pleistocene hominid remains attributed to *Paranthropus* and *Homo* (Broom and Robinson, 1949; Brain, 1970; Robinson, 1970; Susman et al., 2001). Swartkrans was the first site where these two genera were recognized as contemporary. The deposits also include stone artefact assemblages (Leakey, 1970), as well as the earliest evidence of bone culture (Brain et al., 1993) and controlled use of fire by hominids (Brain and Sillen, 1988).

The caves of the Sterkfontein Valley, which were carved in a dolomitic formation of Proterozoic age (the Transvaal Sequence), acted as sedimentary traps and are now filled with calcified breccias. Successive episodes of deposition and erosion have resulted in complex sedimentary accumulations that are particularly difficult to date. Traditional K–Ar and ^{39}Ar–^{40}Ar methods cannot be used because of the lack of contemporaneous volcanic

* Corresponding author. Tel.: +33 4 72 44 58 69; fax: +33 4 72 44 83 82.
E-mail address: Vincent.Balter@univ-lyon1.fr (V. Balter).

0012-821X/$ - see front matter © 2007 Elsevier B.V. All rights reserved.
doi:10.1016/j.epsl.2007.11.039

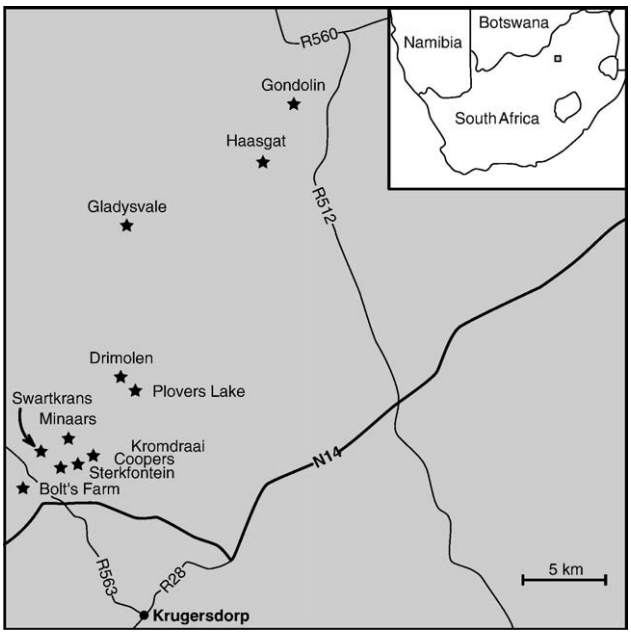

Fig. 1. Map of the main Plio–Pleistocene hominid-bearing sites in the Gauteng Province, South Africa.

fallouts. Other methods have been applied but with variable success. Palaeomagnetic analysis of calcified deposits at Sterkfontein (Partridge et al., 1999) and Kromdraai (Thackeray et al., 2002) exhibits unequivocal changes in polarity. The magnetic sequences were interpreted in terms of age using biochronological calibrations and yielded ages of 3.3 Ma and 1.9 Ma at Sterkfontein and Kromdraai, respectively (Partridge et al., 1999; Thackeray et al., 2002). Absolute dating of sediments at Sterkfontein by means of cosmogenic $^{26}Al/^{10}Be$ gave a mean burial age of 4 Ma for Member 2 (Partridge et al., 2003). This result contrasts with a U–Pb age of 2.2 Ma obtained recently on speleothems from the same locality (Walker et al., 2006).

Fossil teeth from Swartkrans were dated by electron-spin resonance but the broad range of ages obtained turned out to be difficult to interpret (Blackwell, 1994; Curnoe et al., 2001). The current chronology of the deposits, which rests on faunal remains and associated artefacts, also gives conflicting results. Cercopithecoid remains (Delson, 1988) and stone tool assemblages (Clarke, 1993) from each of the three stratigraphic units (hereafter referred to as Member) show no significant age differences and therefore hint at a rapid accumulation. In contrast, bovid (Vrba, 1975, 1985) and equid (Churcher and Watson, 1993) remains suggest an overall time span of 700,000 yr with Members 1, 2, and 3 being consistent with ages of about 1.7, 1.5, and 1.0 Ma, respectively.

The large U/Pb ratios of carbonates have recently been shown very useful for dating speleothems in the Ma range (Walker et al., 2006). The distinct advantage of speleothems for U–Pb dating is their exceedingly high μ ($^{238}U/^{204}Pb$) values (up to 3000), whereas dating the biogenic apatite itself has the payback of providing more direct and thus stronger chronometric evidence of the age of the fossils themselves. The present work explores the potential of U–Pb methods to date fossil apatite. It will be shown that, beyond the analytical difficulties of separating enough Pb to measure and obtain adequate precision on Pb isotope compositions by multi-collector inductively-coupled plasma mass spectrometry (MC-ICP-MS), the conceptual issues associated with the presence of common Pb from different sources and with the U-series disequilibria are arduous. It will also be shown that the isolation of the fossil remains themselves causes serious disruptions of the model assumptions but that a protocol nevertheless can be constructed that helps provide statistically significant ages.

2. The principles of U and Pb uptake and U–Pb chronology

Fossil biogenic phosphates can contain significant amounts of U, typically in the range of 0.1–100 ppm and their μ values are usually very high. Since about 0.015% of the U present in a sample decays into ^{206}Pb every one million years, the potential of the ^{238}U–^{206}Pb chronometer for dating fossil human bones and teeth is strong, even for very young samples. New techniques, notably MC-ICP-MS (Galer, 1999; Albarède et al., 2004), allow for precise correction of instrumental isotopic bias and therefore have greatly improved the precision on young ^{238}U–^{206}Pb ages (Woodhead et al., 2006).

The simplest possible model of U uptake, known as “early uptake” (EU) assumes that U is acquired *post-mortem* during the decay of the organic fraction present in bone material and that subsequently its decay products remained in the host apatite until today (i.e., closed-system behavior). Uptake is supposed to be instantaneous, at least for all practical dating purposes, and the model is not associated with any specific uptake mechanism. One issue, however, may invalidate the EU model: the closed-system assumption does not hold if bones and teeth exchange ^{238}U and nuclides from the decay series such as ^{234}U and ^{230}Th. Such open-system behavior is the rule for diagenesis as well as for recoil emission induced by α-decay, which either drives the daughter nuclides out of the apatite structure or, conversely, from adjacent minerals into it. Emphasis has recently been put on the actual mechanisms of uptake with a diffusion–adsorption model being proposed for U-series dating of fossil bone and teeth (Millard and Hedges, 1996; Pike et al., 2002). The model of “linear uptake” (LU) (Ikeya, 1982; Gallup et al., 1994; Bischoff et al., 1995), which assumes a constant uptake rate of U by fossils, was devised to account for the incorporation of ^{238}U by diffusion, but has been reported to conflict with U profiles obtained by laser-ablation (Eggins et al., 2003). In principle, the initial lack of secular equilibrium between ^{238}U, ^{234}U, and ^{230}Th is an issue of concern for both models, but can be readily handled using the appropriate equations.

For U–Pb dating, Pb isotopic abundances need to be corrected for the presence of common Pb, introduced notably by groundwater and airborne particles, and which cannot be presupposed to be isotopically homogeneous. This problem has important consequences for especially young samples for which the ratio of common to radiogenic Pb is naturally high. Here, we have addressed this matter by assuming that common Pb was introduced as two different components and used the multiplicity of isotopic systems (^{238}U–^{206}Pb, ^{235}U–^{207}Pb,

^{232}Th–^{208}Pb) to break down the mixture of initial Pb into its separate components.

3. Material

Excavations at Swartkrans have revealed that the sedimentary fillings are composed of three main units known as "Members", which are separated from each other by erosional discontinuities (Brain, 1993). The stratigraphically older unit, Member 1, is represented by two distinct deposits, the "Lower Bank" and the "Hanging Remnant" (Fig. 2). The gap between these two deposits was filled with sediments of Members 2 and 3 (Fig. 2).

Lead and U isotope compositions, Pb, U, and Th concentrations, U/Pb ratios, and rare-earth element (REE) concentrations were obtained for enamel samples of indeterminate bovid teeth (Table 1). This material, stored at the Transvaal Museum of Pretoria (South Africa), was excavated from Members 1, 2, and 3, but the exact provenance within each member is unknown.

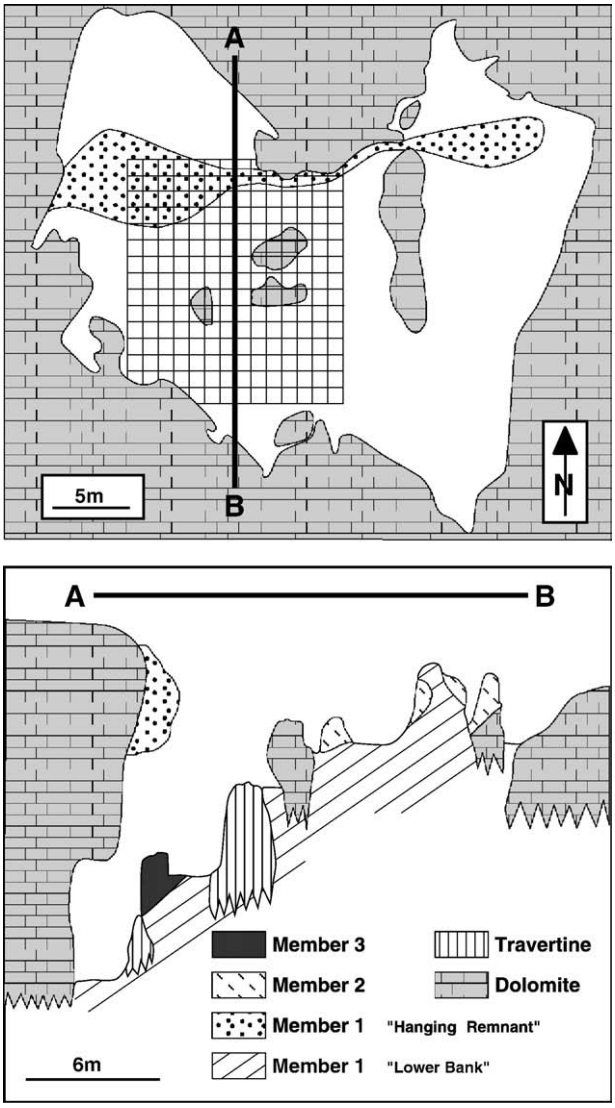

Fig. 2. Map (top panel) and cross-section (bottom panel) of the Swartkrans deposits. The permanent grid of excavation is indicated on the map. Redrawn after Brain (1993).

4. Analytical techniques

Enamel was separated from adjoining dentine using a microdrill and further cleaned for any visible oxy-hydroxide stains. For each sample, between 100 and 300 mg of enamel were ground in an agate mortar and leached with cold 0.1 M acetic acid for one hour. The clean enamel was then dissolved in cold 4.5 M HNO_3. A 50 µl aliquot was taken for U/Pb, Th and REE measurements and the remaining sample solution was processed for Pb isotope analysis. Lead separation was carried out at the Ecole Normale Supérieure in Lyon (ENSL) using anion exchange AG1-X8 (200–400 mesh) micro-columns made from shrink Teflon and employing 0.5 M HBr for sample dissolution, loading of samples onto the columns, and subsequent elution of the sample matrix. 6 M HCl was used to elute the Pb fraction, which was passed through the column twice to ensure maximum Pb purity for optimal mass spectrometric analysis. Total procedural Pb blanks were better than 25 pg for all sample batches. Pb isotopic compositions were measured at ENSL in static mode by MC-ICP-MS using either the VG Plasma 54 or the Nu Plasma HR both coupled with a desolvating nebulizer (an Aridus for the Plasma 54 and a Nu DSN-100 for the Nu Plasma). The Tl doping and standard bracketing method was used to correct for instrumental mass fractionation (White et al., 2000; Albarède et al., 2004). U/Pb ratios and REE and Th concentrations were measured by quadrupole ICP-MS (X7, ThermoElemental) at ENSL, using In as the internal standard.

The need for U isotope analyses in addition to the Pb isotope measurements developed during the course of the present project and the measurements were done on eight separate enamel samples, which were leached as described above. The procedure was repeated three times for the samples "M2", "M3-36230", and "M3-38065" leading to three successive leachates (see Table 2). Uranium separation was carried out at ENSL using anion exchange AG1-X8 (100–200 mesh) Biorad© columns. 6 M HCl was employed for sample dissolution, loading onto the columns, and subsequent elution of the sample matrix. 1 M HCl was used to elute the U fraction. Uranium isotopic compositions were measured on the Nu Plasma HR coupled with the Nu DSN-100 desolvating nebulizer and using the standard bracketing method to correct for instrumental mass fractionation (White et al., 2000; Albarède et al., 2004). Precision on the measurements of ^{234}U/^{238}U typically is of the order of 0.5 permil. The total procedural U blank was better than 1 pg.

5. Results

The average U content of the teeth (0.74±0.34 µg/g) is one order of magnitude higher than the U concentration of fresh bone (0.07 µg/g) (Table 1) (Hinners et al., 1998). The total REE concentrations and $(La/Sm)_N$ ratio range from 0.01 to 2.37 µg/g and 0.52 to 1.58, respectively (Table 1). Concentrations are not noticeably different between the different Members.

Table 1
REE, Pb, U and Th concentrations, La/Sm ratios, and Pb isotope compositions for the samples from Swartkrans and the NIST standard SRM1400

	Rare earth elements (NASC normalized)[a]																			
	La	Ce	Pr	Nd	Sm	Gd	Tb	Dy	Ho	Er	Tm	Yb	Lu	$(La/Sm)_N$	$(\Sigma REE)_N$[a]	Pb[a]	U[a]	Th[a]	$^{238}U/^{206}Pb$[b]	$^{204}Pb/^{206}Pb$	$^{207}Pb/^{206}Pb$
Swartkrans Member 1																				
M1-5359a	0.002	0.001	0.001	0.001	0.001	0.001	0.001	0.001	0.001	0.001	0.001	0.001	0.002	1.58	0.02	0.11	0.55		18.0±0.3	0.048660±2	0.781144±18
M1-5359b	0.001	0.001	0.002	0.001	0.002	0.002	0.006	0.002	0.005	0.002	0.008	0.002	0.010	0.65	1.31	0.14	0.23		5.4±0.2	0.048661±3	0.780465±12
M1-5806	0.015	0.004	0.012	0.012	0.013	0.014	0.013	0.013	0.014	0.014	0.014	0.016	0.017	1.16	0.17	0.25	1.6		21.7±0.7	0.052520±3	0.824988±11
M1-13892a																0.08	0.72	0.01	35.5±0.5	0.053817±6	0.839695±54
M1-13892b	0.002	0.001	0.002	0.001	0.002	0.002	0.007	0.002	0.005	0.002	0.008	0.002	0.011	0.94	0.05	0.25	0.68		9.3±0.2	0.053038±2	0.833510±8
M1-12495a																0.12	0.67		19.5±0.4	0.052156±5	0.821147±12
M1-12495b																0.11	0.66	0.04	25.0±0.4	0.052095±10	0.820917±52
M1-12495c																0.14	0.57	0.14	16.4±0.3	0.052253±7	0.822554±46
Swartkrans Member 2																					
M2-M2a																0.14	0.93	0.03	27.3±0.3	0.053642±7	0.839743±46
M2-M2b	0.001	0.000	0.001	0.001	0.001	0.001	0.001	0.001	0.001	0.001	0.001	0.001	0.001	1.56	0.01	0.09	1.2		50.9±1.5	0.052696±6	0.826527±11
M2-1272a	0.001	0.000	0.001	0.001	0.001	0.001	0.001	0.001	0.001	0.001	0.001	0.001	0.003	1.56	0.01	0.13	2.3		62.4±1.3	0.054415±2	0.847240±7
M2-1272b																0.17	2.4	0.19	58.4±1.0	0.054563±8	0.849097±57
M2-1272c																0.21	2.8	0.02	53.9±1.1	0.054412±4	0.847959±26
M2-2619	0.001	0.000	0.001	0.001	0.001	0.002	0.002	0.001	0.002	0.002	0.002	0.002	0.004	1.15	2.12	0.08	0.93		39.8±1.0	0.053122±2	0.831798±

(continued on next page)

Table 1 (*continued*)

	Rare earth elements (NASC normalized)[a]																			
	La	Ce	Pr	Nd	Sm	Gd	Tb	Dy	Ho	Er	Tm	Yb	Lu	$(La/Sm)_N$	$(\Sigma REE)_N$[a]	Pb[a]	U[a]	Th[a]	$^{238}U/^{206}Pb$[b]	$^{204}Pb/^{206}Pb$	$^{207}Pb/^{206}Pb$
M2-2916a	0.012	0.002	0.011	0.012	0.012	0.014	0.012	0.012	0.012	0.013	0.011	0.012	0.0137	1.03	2.19	0.10	0.87		29.5±0.6	0.053756±2	7 0.840494±8
M2-2916b																0.10	2.2	0.02	90.5±1.7	0.052131±10	0.817981±96
M2-3705a	0.002	0.001	0.002	0.002	0.002	0.002	0.003	0.002	0.002	0.002	0.002	0.002	0.005	0.98	2.37	0.13	0.91		23.5±0.9	0.052589±3	0.826169±16
M2-3705b																0.15	0.52	0.04	14.3±0.3	0.052652±9	0.828172±64
Swartkrans Member 3																					
M3-34459	0.016	0.007	0.013	0.012	0.013	0.010	0.010	0.009	0.009	0.008	0.007	0.007	0.007	1.28	0.13	0.38	2.5		23.1±0.4	0.047056±2	0.761880±8
M3-34946	0.081	0.005	0.119	0.134	0.155	0.176	0.132	0.125	0.137	0.124	0.104	0.107	0.098	0.52	1.50	0.16	3.7		87.9±1.2	0.051800±4	0.816171±13
M3-30375	0.000	0.000	0.000	0.000	0.000	0.000	0.001	0.000	0.000	0.001	0.001	0.001	0.001	1.01	0.01	0.05	0.32		20.1±0.3	0.051341±2	0.812817±6
M3-36803	0.005	0.000	0.004	0.005	0.005	0.006	0.005	0.004	0.004	0.004	0.003	0.004	0.007	0.92	0.06	0.07	1.7		82.6±3.0	0.052804±2	0.828679±9
M3-38065	0.020	0.003	0.023	0.026	0.029	0.030	0.024	0.020	0.021	0.018	0.017	0.016	0.018	0.69	0.27	0.17	1.2		23.5±0.7	0.054109±4	0.846527±15
													Total	1.07 ±0.34	0.73 ±0.94						
																			$^{208}Pb/^{204}Pb$	$^{206}Pb/^{204}Pb$	$^{207}Pb/^{206}Pb$
SRM-1400 "Bone Ash" ($n=3$)																					
Mean±sd	0.010	0.009	0.008	0.009	0.008	0.006	0.010	0.009	0.009	0.008	0.009	0.006	0.009	1.24	0.11	8.3	0.068		38.663	18.377	0.85362
	0.000	0.000	0.000	0.001	0.004	0.005	0.004	0.002	0.004	0.002	0.003	0.002	0.006			2.0	0.004		0.001	0.001	0.00001
Reported values[c]																					
Mean (Lab. C)	0.010	0.010	0.010	0.009	0.011	0.014	0.012	0.009	0.012	0.008	0.006	0.007	<0.015	0.97	0.13	9	0.066		38.610	18.3676	0.85314
±sd (Lab. C)	0.001	0.001	0.001	0.001	0.001	0.001	0.001	0.001	0.004	0.001	0.001	0.002							0.052	0.0380	0.00870

[a] Unit in μg/g.

Table 2
U isotope compositions (activity ratios) for residual enamel (R) and the corresponding leachate (L)

	$^{234}U/^{238}U$
Swartkrans Member 1	
M1-5359R	1.3679±8
M1-5359L	1.0551±12
M1-5806R	1.2678±6
M1-5806L	1.0230±11
M1-12495R	1.1168±5
M1-12495L	0.9053±5
M1-12710R	1.3455±10
M1-12710L	1.2712±22
M1-13892R	1.2239±6
M1-13892L	1.2374±40
Swartkrans Member 2	
M2R	1.2464±7
M2-L	1.3647±10
M2-L2	1.4109±26
M2-L3	1.2389±21
Swartkrans Member 3	
M3-36230R	1.3339±7
M3-36230L	1.2190±24
M3-36230L2	0.9531±3
M3-36230L3	1.0468±16
M3-38065R	1.1589±8
M3-38065L	1.2258±12
M3-38065L2	1.1507±23
M3-38065L3	1.0670±18

Suffixes L2 and L3 stand for a second and a third leachate.

The μ values are, as expected, very high, and vary between 100 and 1700 with a mean value of 400. The $^{207}Pb/^{204}Pb$ data scatter (15.8%, RSD) well beyond analytical uncertainties and what can be expected from radiogenic ingrowth (10 ppm per million years). In a plot of $^{207}Pb/^{204}Pb$ vs $^{206}Pb/^{204}Pb$ the data form an alignment with a slope of ~0.21, which cannot be associated with a meaningful age and therefore is not a secondary isochron (Fig. 3). Each Member alone forms an alignment consistent with the overall trend. The spread of the data is similar from one Member to another with Member 2 missing the most radiogenic value. The common crustal Pb represented by the values of Stacey and Kramers (1975) (18.70 and 15.63) plots near the lower part of the Swartkrans trend.

Our ^{234}U data show a ~26% excess over ^{238}U (Table 2) consistent with the values previously observed by Curnoe et al. (2001) on unleached samples. The $[^{234}U/^{238}U]$ activity ratio is up to 30% higher in residual enamel with respect to the corresponding leachate (Table 2).

6. Discussion

The scatter of Pb isotopic compositions indicates that the alignment in the $^{207}Pb/^{204}Pb$ vs $^{206}Pb/^{204}Pb$ plot cannot be associated with a geologically meaningful age and therefore is a mixing line. Two prominent end-members of this mixing line are (i) unradiogenic Pb similar to the ubiquitous common crustal Pb of Stacey and Kramers (1975), and (ii) radiogenic Pb most likely inherited from the Archean crystalline basement or the overlying Proterozoic carbonates. With the Pb in the present samples being dominated by common Pb, the question arises of when uptake of trace elements took place and, in particular, whether protracted interaction between enamel and percolating fluids (late diagenesis) was important or not.

A first hint is provided by the REE concentrations: REEs tend to accumulate in bioapatite during diagenesis through adsorption. When diagenesis lasts long enough, however, they ultimately fractionate in favor of the intermediate REEs resulting in a "bell-shaped" spectrum (Reynard et al., 1999) with $(La/Sm)_N \ll 1$. Because in the present samples the $(La/Sm)_N$ ratios are ~1 and similar to $(La/Sm)_N$ of fresh bone, we conclude that late diagenesis either did not take place or was of only short duration. This is consistent with the apparent similarity of the total REE contents (~0.1 μg/g) with REE contents measured in fresh material (Hinners et al., 1998).

The case for U is more complicated because this element is much more soluble than REEs and therefore more susceptible to prolonged episodes of loss and uptake. Its much larger concentrations in the fossil enamel of the present samples with respect to fresh material indicate that the overall U uptake has been quite efficient. The chronological potential of the U–Pb chronometer therefore depends on the history of U uptake by apatite. In order to interpret the data, we will first establish the constitutive equations of the two models of early uptake and linear uptake/loss when initial Pb is a mixture of separate components. Particular attention has been paid to the uptake of U descendents in order for U-disequilibrium data to be used to validate a given model.

6.1. The "early uptake" U–Pb chronometer with two common Pb components

Even for material apparently immune to late diagenesis, the issue of initial isotopic homogeneity of common Pb remains

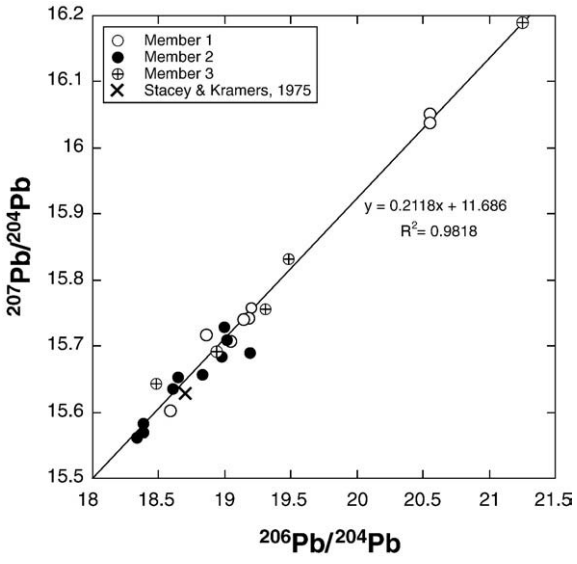

Fig. 3. Plot of $^{207}Pb/^{204}Pb$ vs $^{206}Pb/^{204}Pb$ for the samples analyzed in this study. The value of common Pb as calculated by Stacey and Kramers (1975) is shown for reference.

problematic, since, contrary to igneous rocks, no thermally-induced isotopic homogenization has taken place. We have addressed this issue by assuming that at age t_0, the system incorporated U and two common Pb components, (typically old Precambrian Pb from the basement and young Pb from surface sediments), labeled α_0^1 and α_0^2, in the proportions f and $1-f$. For the ^{238}U–^{206}Pb system, mass balance after time t reads:

$$\left(\frac{^{206}\mathrm{Pb}}{^{204}\mathrm{Pb}}\right)_t = f\alpha_0^1 + (1-f)\alpha_0^2 + \left(\frac{^{238}\mathrm{U}}{^{204}\mathrm{Pb}}\right)_t \left(e^{\lambda_{238U}t} - 1\right) + \frac{^{234}\mathrm{U}_{xs,0}}{^{204}\mathrm{Pb}} - \frac{^{230}\mathrm{Th}_{\mathrm{sec}}}{^{204}\mathrm{Pb}} \quad (1)$$

where the subscripts xs,0 and sec stand for initial excess and secular, respectively. In this equation, we have neglected loss and uptake of nuclides in the decay series with mass numbers lower than that of ^{230}Th on the grounds that they are turned into Pb faster than they can be incorporated into the phosphate. We also neglected the initial uptake of ^{230}Th and ^{234}Th on the grounds that Th/U of phosphates is very low (0.06±0.08, Table 1). The second to last term represents the accumulation of radiogenic ^{206}Pb due to initial ^{234}U excess, while the last term represents the build-up of ^{230}Th to its secular equilibrium value from the decay of its parent isotopes. Similarly, for the ^{235}U–^{207}Pb system:

$$\left(\frac{^{207}\mathrm{Pb}}{^{204}\mathrm{Pb}}\right)_t = f\beta_0^1 + (1-f)\beta_0^2 + \left(\frac{^{235}\mathrm{U}}{^{204}\mathrm{Pb}}\right)_t \left(e^{\lambda_{235U}t} - 1\right) + \frac{^{231}\mathrm{Pa}_{xs,0}}{^{204}\mathrm{Pb}} \quad (2)$$

The assumptions here are similar to those just made for Eq. (1), except that ^{231}Pa incorporation is considered. The parameter f is obtained from Eq. (1) as:

$$f\left(\alpha_0^2 - \alpha_0^1\right) = \left(\frac{^{206}\mathrm{Pb}}{^{204}\mathrm{Pb}}\right)_t - \alpha_0^1 - \left(\frac{^{238}\mathrm{U}}{^{204}\mathrm{Pb}}\right)_t \times \left(e^{\lambda_{238U}t} - 1 + \frac{^{234}\mathrm{U}_{xs,0}}{^{238}\mathrm{U}} - \frac{\lambda_{238U}}{\lambda_{230Th}}\right) \quad (3)$$

Introducing the previous equation into Eq. (2), and neglecting the $^{231}\mathrm{Pa}_{xs,0}/^{204}$Pb term gives:

$$\frac{\alpha_0^2 - \alpha_0^1}{\beta_0^2 - \beta_0^1}\left[\left(\frac{^{207}\mathrm{Pb}}{^{204}\mathrm{Pb}}\right)_t - \beta_0^1\right] = \left(\frac{^{206}\mathrm{Pb}}{^{204}\mathrm{Pb}}\right)_t - \alpha_0^1 - \left(\frac{^{238}\mathrm{U}}{^{204}\mathrm{Pb}}\right)_t \times \left(e^{\lambda_{238U}t} - 1 - \frac{\alpha_0^2 - \alpha_0^1}{\beta_0^2 - \beta_0^1}\frac{e^{\lambda_{235U}t} - 1}{137.88} + \frac{^{234}\mathrm{U}_{xs,0}}{^{238}\mathrm{U}} - \frac{\lambda_{238U}}{\lambda_{230Th}}\right) \quad (4)$$

In order to minimize correlations between variables, we switch to normalization to ^{206}Pb by multiplying the previous equation by ^{204}Pb/^{206}Pb. Moreover, using the approximation $e^{\lambda t} - 1 \approx \lambda t$, valid for both ^{238}U and ^{235}U for which $\lambda t \ll 1$, we finally obtain:

$$\frac{\alpha_0^1\beta_0^2 - \alpha_0^2\beta_0^1}{\beta_0^2 - \beta_0^1}\left(\frac{^{204}\mathrm{Pb}}{^{206}\mathrm{Pb}}\right)_t + \frac{\alpha_0^2 - \alpha_0^1}{\beta_0^2 - \beta_0^1}\left(\frac{^{207}\mathrm{Pb}}{^{206}\mathrm{Pb}}\right)_t + \left(\frac{^{238}\mathrm{U}}{^{206}\mathrm{Pb}}\right)_t \times \left(\lambda_{238U}t - \frac{\alpha_0^2 - \alpha_0^1}{\beta_0^2 - \beta_0^1}\frac{\lambda_{235U}t}{137.88} + \frac{^{234}\mathrm{U}_{xs,0}}{^{238}\mathrm{U}} - \frac{\lambda_{238U}}{\lambda_{230Th}}\right) = 1 \quad (5)$$

which can be simplified as:

$$m\left(\frac{^{204}\mathrm{Pb}}{^{206}\mathrm{Pb}}\right)_t + n\left(\frac{^{207}\mathrm{Pb}}{^{206}\mathrm{Pb}}\right)_t + s(t)\left(\frac{^{238}\mathrm{U}}{^{206}\mathrm{Pb}}\right)_t = 1 \quad (6)$$

with:

$$m = \frac{\alpha_0^1\beta_0^2 - \alpha_0^2\beta_0^1}{\beta_0^2 - \beta_0^1} \quad (7)$$

and:

$$n = \frac{\alpha_0^2 - \alpha_0^1}{\beta_0^2 - \beta_0^1} \quad (8)$$

and:

$$s(t) = \left[\left(\lambda_{238U} - n\frac{\lambda_{235U}}{137.88}\right)t + \frac{^{234}\mathrm{U}_{xs,0}}{^{238}\mathrm{U}} - \frac{\lambda_{238U}}{\lambda_{230Th}}\right]. \quad (9)$$

If the $^{234}\mathrm{U}_{xs,0}/^{238}$U ratio is constant for all the samples analyzed, i.e., constant in the aquifer which acted as the source of U, there is one linear equation in m, n, and s per sample, m and n being constants and $s(t)$ a known function of time t. From the Pb isotopic compositions and the U/Pb ratios, the system can be solved for the three unknowns and thus for t. Each equation is weighted using the full correlation matrix of the variables. The sum of squared residuals on ^{207}Pb/^{206}Pb is solved using a standard non-linear minimization algorithm provided by MatLab. The age uncertainties were calculated using Monte Carlo techniques.

The ^{232}Th–^{208}Pb system gives two additional equations similar to Eq. (4):

$$\frac{\alpha_0^2 - \alpha_0^1}{\gamma_0^2 - \gamma_0^1}\left[\left(\frac{^{208}\mathrm{Pb}}{^{204}\mathrm{Pb}}\right)_t - \gamma_0^1\right] = \left(\frac{^{206}\mathrm{Pb}}{^{204}\mathrm{Pb}}\right)_t - \alpha_0^1 - \left(\frac{^{238}\mathrm{U}}{^{204}\mathrm{Pb}}\right)_t \times \left(e^{\lambda_{238U}t} - 1 + \frac{^{234}\mathrm{U}_{xs,0}}{^{238}\mathrm{U}} - \frac{\lambda_{238U}}{\lambda_{230Th}}\right) \quad (10)$$

and:

$$\frac{\beta_0^2 - \beta_0^1}{\gamma_0^2 - \gamma_0^1}\left[\left(\frac{^{208}\mathrm{Pb}}{^{204}\mathrm{Pb}}\right)_t - \gamma_0^1\right] = \left(\frac{^{207}\mathrm{Pb}}{^{204}\mathrm{Pb}}\right)_t - \beta_0^1 - \frac{1}{137.88}\left(\frac{^{238}\mathrm{U}}{^{204}\mathrm{Pb}}\right)_t \left(e^{\lambda_{235U}t} - 1\right) \quad (11)$$

where γ_0^1 and γ_0^2 stand for two initial ^{208}Pb–^{204}Pb components. The method can be extended to three Pb components by using the three radiogenic systems simultaneously, which of course produces more cumbersome equations. Anticipating the rest of the discussion, however, we assert already here that the 3-component assumption does not lead to significantly different results nor does it improve the mean-squared weighted deviation (most likely because of the slow production of ^{208}Pb) and therefore will not be considered further (see online Appendix A).

6.2. The "linear uptake" U–Pb chronometer

The radioactive U–Pb systems may be open because of continuous uptake of nuclides from ambient water and continuous loss by recoil. U-series disequilibria have been dealt with for open-system models by a number of authors who among them used a variety of different assumptions. Gallup et al. (1994) and Bischoff et al. (1995) assumed a constant uptake rate of nuclides from the interstitial fluids by the host phase. Henderson and Slowey (2000), Villemant and Feuillet (2003), and Thompson et al. (2003) considered that loss by α-recoil is proportional to the number of decaying nuclides.

Our new model is described in detail in the online Appendix B. First, we observe that the recoil distance is determined by the particular energetics of the decay reaction and by the property of the solid phase and is of the order of 40 nm (Harvey, 1962). To a large extent, the fraction of recoiling nuclide therefore is controlled not only by the volume but also by the surface area of the apatite crystallites. Consequently, we will not assume that loss by recoil and uptake are proportional to the amount of available nuclides, but rather that they can be described by constant j_{238}, j_{234}, and j_{230} fluxes for ^{238}U, ^{234}U, and ^{230}Th, respectively (^{234}Th is neglected). Given the range of ^{238}U and ^{234}U concentrations, it is not expected that the different assumptions are critical to these two nuclides. These parameters, which lump together all the fluxes between the interstitial fluid and the solid phase regardless of the process, are positive for linear uptake and negative for α-recoil processes. We also assume that $e^{-\lambda_{230}t}$ and $e^{-\lambda_{234}t}$ are negligibly small, a condition we loosely refer to as 'secular equilibrium' even if this term usually applies to a closed system. The system of differential equations, written with activity ratios, is:

$$\frac{d}{dt}\begin{bmatrix}[^{238}U]\\ [^{234}U]\\ [^{230}Th]\end{bmatrix} = \begin{bmatrix}-\lambda_{238} & 0 & 0\\ \lambda_{234} & -\lambda_{234} & 0\\ 0 & \lambda_{230} & -\lambda_{230}\end{bmatrix}\begin{bmatrix}[^{238}U]\\ [^{234}U]\\ [^{230}Th]\end{bmatrix} + \begin{bmatrix}\lambda_{238}j_{238}\\ \lambda_{234}j_{234}\\ \lambda_{230}j_{230}\end{bmatrix} \quad (12)$$

where λ_{238}, λ_{234}, and λ_{230} are the decay constants of ^{238}U, ^{234}U, and ^{230}Th, respectively. The model provides the activity of the major U-series nuclides as:

$$[^{234}U]_{sec} - [^{238}U]_{sec} = \left(1 - e^{-\lambda_{238}t}\right)j_{234} \quad (13)$$

$$[^{230}Th]_{sec} - [^{234}U]_{sec} = \left(1 - e^{-\lambda_{238}t}\right)j_{230}. \quad (14)$$

A general expression for the open-system production of total ^{206}Pb at secular equilibrium (t_s) is derived as:

$$^{206}Pb(t_s) - {}^{206}Pb(0) = {}^{238}U_{sec}\left(\lambda_{238}t_s + [^{230}Th]_{xs}\right) \quad (15)$$

where $^{238}U_{sec}$ is the number of atoms of ^{238}U at secular equilibrium and $[^{230}Th]_{xs}$ the excess activity of ^{230}Th. The effects of ^{238}U decay and diagenesis on the total production of ^{206}Pb are represented by $\lambda_{238}t_s$ and $[^{230}Th]_{xs}$, respectively. Dividing this equation by ^{204}Pb gives:

$$\left(\frac{^{206}Pb}{^{204}Pb}\right)_{t_s} - \left(\frac{^{206}Pb}{^{204}Pb}\right)_0 = \left(\frac{^{238}U}{^{204}Pb}\right)_{t_s}\left(\lambda_{238}t_s + [^{230}Th]_{xs}\right). \quad (16)$$

6.3. The age of Swartkrans fossils

Before we attempt to use the U–Pb chronometer described above, the first issue to be addressed is to assess the implications of disequilibrium among U-series nuclides. Apparently, although we will see that this is not an acceptable interpretation, disequilibrium between ^{234}U and ^{238}U seems to invalidate the early uptake model. However, the contrast between the 20–30% excess of ^{234}U found both by Curnoe et al. (2001) and in the present study (Table 2) and the conspicuous secular equilibrium between ^{230}Th and ^{234}U in the same material ($[^{230}Th/^{234}U]=0.970\pm0.102$) is particularly puzzling. If the model of linear uptake holds, equal ^{230}Th and ^{234}U activities require that $[^{230}Th]_{xs}=[^{234}U]_{xs}\sim0.3$ (Table 2 in Curnoe et al., 2001, and our Table 2). When combined with the very high μ values observed in enamel, typically 400, the last term of Eq. (16) indicates that such a large excess should increase the $^{206}Pb/^{204}Pb$ ratio to extremely high values ($\sim400\times0.3=120$). Such an extreme isotopic variability definitely is not observed in the $^{206}Pb/^{204}Pb$ ratios of the present samples, thereby demonstrating the lack of ^{230}Th excess and raising the question of how values of $[^{234}U/^{238}U]>1$ originated in the first place.

The most likely explanation for excess ^{234}U is that it was created during initial sample preparation. If recoil transports ^{234}U out of apatite, preferential leaching of this nuclide is to be expected compared to its parent ^{238}U. The data clearly contradict this prediction since ^{234}U excesses of up to 30% are observed in the residue with respect to the leachates. The data therefore rather indicate that a labile part of ^{238}U hosted in pores was preferentially removed by sample processing, whereas the daughter products had recoiled into the phosphate lattice and thereby become immune to leaching. Fossil biogenic carbonate hydroxylapatite thus may be considered a dual U reservoir. One reservoir hosts uranyl-carbonate complexes absorbed from oxic groundwater (Morse et al., 1984), while the other, consisting of presumably reduced U^{4+}, remains in the pores left by the decay of organic material. The two reservoirs react differently to the decalcification step routinely used to extract fossils from the breccias. Out of a total loss of ~26%, which is the mean value of the $^{234}U_{xs}$ of residues (Table 2), ~6% of the ^{238}U loss can be ascribed to the leaching step intended to clean up the enamel for

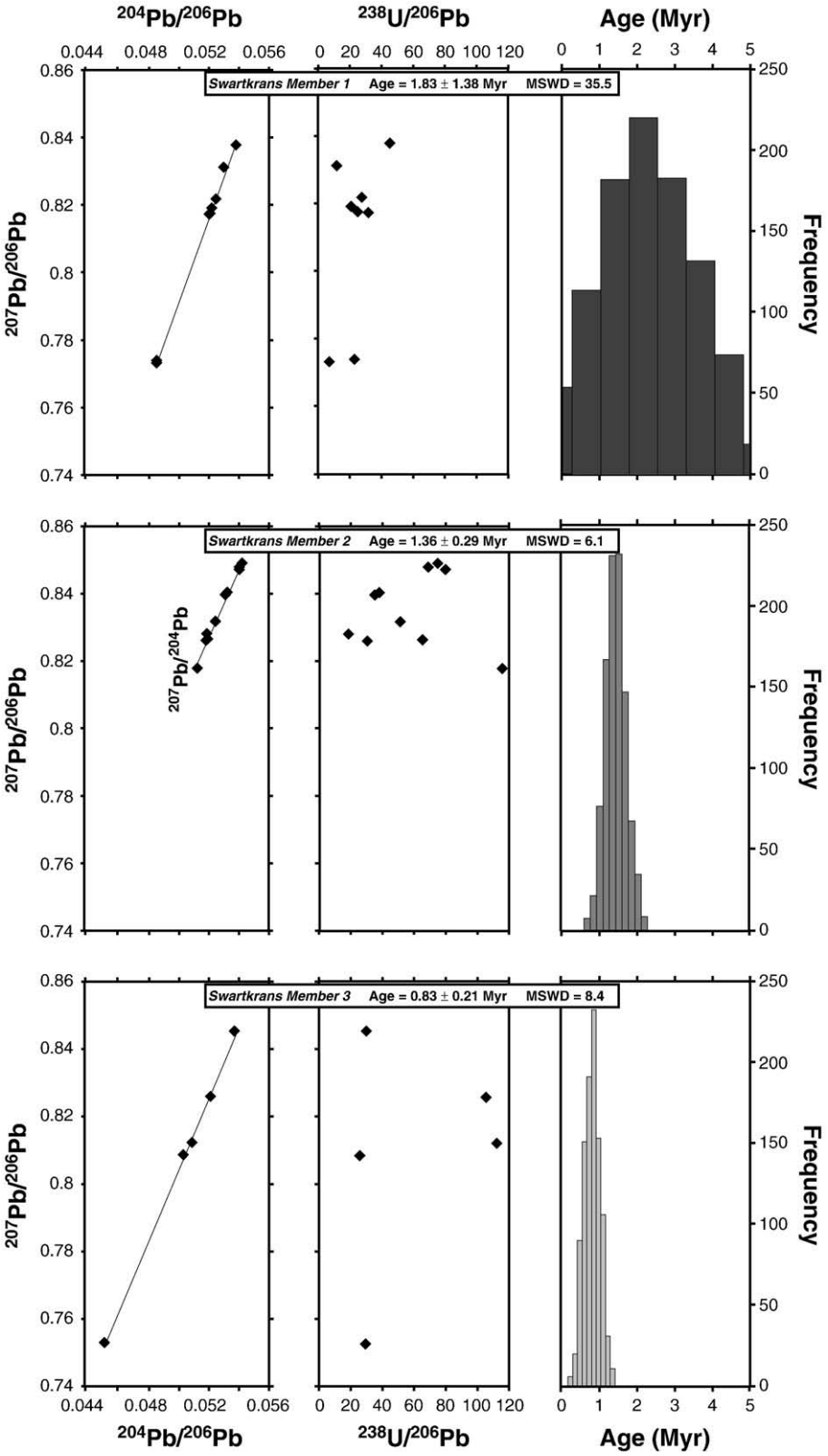

Fig. 4. $^{207}Pb/^{206}Pb$–$^{204}Pb/^{206}Pb$ and $^{207}Pb/^{206}Pb$–$^{238}U/^{206}Pb$ distributions and corresponding age frequency histograms obtained for the three Members of Swartkrans. Ages are calculated by minimization of the error-weighted chi-squared sum of squared residuals. The histograms were obtained via Monte Carlo simulation (1000 runs) using random deviates corresponding to the uncertainties on the $^{238}U/^{206}Pb$, $^{207}Pb/^{206}Pb$, and $^{204}Pb/^{206}Pb$ ratios. The quoted range of errors covers 95% of the outcomes. The initial groundwater $^{234}U/^{238}U$ activity ratio is ~2 (Walker et al., 2006). $^{207}Pb/^{206}Pb$ and $^{204}Pb/^{206}Pb$ ratios are associated with external errors of 300 ppm and 100 ppm, respectively. The decay constants values used for ^{238}U, ^{235}U, ^{234}U, and ^{230}Th are $0.155125\times10^{-9}yr^{-1}$, $0.98485\times10^{-9}yr^{-1}$, $2.79\times10^{-6}yr^{-1}$, and $9.21\times10^{-9}yr^{-1}$, respectively.

Pb isotope analysis, leaving ~20% for the decalcification (extraction) step. In the process, [^{230}Th]/[^{234}U] is left unchanged because recoil propelled both daughter nuclides into solid apatite.

We hence conclude that the early uptake model is adequate for chronometric interpretation of the present data provided the ^{238}U activities are readjusted to match the ^{234}U activities. In essence, loss of ^{238}U during sample preparation suggests that the ^{234}U–^{206}Pb chronometer should be used instead of the conventional ^{238}U–^{206}Pb pair. The relative age correction exactly reflects the relative ^{238}U loss, i.e., 10 ka per Ma and per percent of ^{238}U loss. We therefore used Eqs. (6)–(9) of the chronometer with two common Pb components as described above. Without ^{238}U correction, the apparent ages would be 2.67±1.58 Ma for Member 1, 1.74±0.41 Ma for Member 2, and 1.12±0.25 Ma for Member 3. Correcting the present data for a 26% ^{238}U loss leads to the final ages of 1.83±1.38 Ma for Member 1, 1.36±0.29 Ma for Member 2, and 0.83±0.21 Ma for Member 3 (Fig. 4).

The ages obtained also depend on the initial U isotopic composition of the samples, which, in turn, is equal to the ^{234}U/^{238}U value of the aquifer. Although large variations of ^{234}U disequilibrium have been reported by Kronfeld et al. (1994) in the Transvaal dolomite aquifer, Walker et al. (2006) calculated an initial ^{234}U excess value of 100% for a 2.2 Ma old speleothem at Sterkfontein. This is the value we used for our calculations on the grounds that Sterkfontein and Swartkrans are distant by only few hundreds of meters and that their activity overlapped in time. Such a value is also representative of the average value of modern surface waters of southern Africa (Kronfeld and Vogel, 1991). The ±20% range of $^{234}U_{xs}$ variations reported by these authors corresponds to an uncertainty of 90 ka on the ages.

7. Implications for hominid evolution in South Africa

The much larger uncertainty on the age of Member 1 is due largely to the lack of high-^{238}U/^{204}Pb samples, which reflects continuous uptake of common Pb during diagenesis. Despite the poor precision on this age, the overall temporal sequence deduced from the isotopic data obtained in this study fits the pattern established by biochronological observations (Vrba, 1975, 1985; Churcher and Watson, 1993) with different ages for the three members within an overall time span of about one million years. At Swartkrans, fossil hominids attributed to *Homo* are represented by abundant cranio-dental remains in Members 1 and 2 but by post-cranial remains only in Member 3. The consistency between bio- and radio-chronological time scales indicates that these fossils represent either one single species living over almost one million years, or diverse species of *Homo* clearly separated in time, but which still need to be properly identified. This is the case, for instance, for several cranio-dental remains found in Member 3 that were first assigned by J.T. Robinson to a new genus, *Telanthropus*, but subsequently referred to as *H. erectus s.l.* (Robinson, 1953). Taking the oldest *P. boisei/H. habilis* assemblage of the Omo Shungura Formation in Kenya (White, 1988), which is dated at 2.3 Ma, into account, coexistence of *Paranthropus* and *Homo* over 1.5 Ma is consistent with the present data.

8. Conclusions

We have shown that fossil enamel can be dated with the use of models of early U uptake with multiple initial Pb components. Radiogenic Pb only starts accumulating when U is introduced from ambient groundwater but, common – or initial – Pb is also incorporated at this stage and needs to be corrected for in order to reach radiogenic Pb. The Pb isotopic composition is thus broken down into its separate components using the multiplicity of U–Th/Pb isotopic systems. With respect to U uptake, we affirm that continuous redistribution of ^{238}U, ^{234}U, and ^{230}Th exists between apatite and pore water, which is controlled by α-recoil processes and diagenetic exchanges, and propose a new model that accounts for both of these mechanisms.

This model was applied to a suite of U–Pb isotopic compositions of well-preserved bovid enamel samples excavated from the Swartkrans Pleistocene hominid site in South Africa. After a ~30% correction for ^{238}U loss and an initial groundwater ^{234}U disequilibrium of 100% (Walker et al., 2006), the U–Pb chronometer yields ages of 1.83±1.38, 1.36±0.29, and 0.83±0.21 Ma, for Members 1, 2, and 3, respectively, which are in very good agreement with the observed biochronological time frame.

The present study is the first to have acquired reliable radiometric data directly on fossil bioapatite of an age beyond the range of the U-series method, thus opening up perspectives for the construction of an unequivocal time frame of early hominid evolution that may include both Central, East, and South Africa.

Acknowledgements

This work was supported by the South African National Research Foundation, the French Ministry of Foreign Affairs, the French Embassy in South Africa through the Cultural and Cooperation Services, and the French Institut National des Sciences de l'Univers through the program ECLIPSE II. Many thanks are due to the Northern Flagship Institution, the South African Heritage Resources Agency, and the Transvaal Museum for facilitating the access to the fossil samples. We further thank Tim Partridge and an anonymous reviewer for useful comments. This is contribution UMR5125-07.060.

Appendix A. Supplementary data

Supplementary data associated with this article can be found, in the online version, at doi:10.1016/j.epsl.2007.11.039.

References

Albarède, F., Telouk, P., Blichert-Toft, J., Boyet, M., Agranier, A., Nelson, B., 2004. Precise and accurate isotopic measurements using multiple-collector ICPMS. Geochim. Cosmochim. Acta 68, 2725–2744.

Bischoff, J.L., Rosenbauer, R.J., Moensch, A.F., Ku, T.-L., 1995. Uranium series age equations for uranium assimilation by fossil bone. Radiochim. Acta 69, 127–135.

Blackwell, B.A., 1994. Problems associated with reworked teeth in electron spin resonance (ESR) dating. Quat. Sci. Rev. 13, 651–660.

Brain, C.K., 1970. New finds at the Swartkrans Australopithecines Site. Nature 225, 1112–1119.
Brain, C.K., 1993. Structure and stratigraphy of the Swartkrans Cave in the light of the new excavations. In: Brain, C.K. (Ed.), A Cave's Chronicle of Early Man. Transvaal Museum Monograph, Pretoria, pp. 23–33.
Brain, C.K., Shipman, P., 1993. The Swartkrans bone tools. In: Brain, C.K. (Ed.), A Cave's Chronicle of Early Man. Transvaal Museum Monograph, Pretoria, pp. 195–215.
Brain, C.K., Sillen, A., 1988. Evidence from the Swartkrans cave for the earliest use of fire. Nature 336, 464–466.
Broom, R., Robinson, J.T., 1949. A new type of fossil man. Nature 164, 322.
Churcher, C.S., Watson, V., 1993. Additional fossil equidae from Swartkrans. In: Brain, C.K. (Ed.), A Cave's Chronicle of Early Man. Transvaal Museum Monograph, Pretoria, pp. 137–150.
Clarke, J.D., 1993. Stone artefact assemblages from Members 1–3, Swartkrans Cave. In: Brain, C.K. (Ed.), A Cave's Chronicle of Early Man. Transvaal Museum Monograph, Pretoria, pp. 167–194.
Curnoe, D., Grün, R., Taylor, L., Thackeray, F., 2001. Direct ESR dating of a Pliocene hominin from Swartkrans. J. Hum. Evol. 40, 379–391.
Delson, E., 1988. Chronology of South African australopith site units. In: Grine, F.E. (Ed.), Evolutionary History of the 'Robust' Australopithecines. Aldine de Gruyter, New York, pp. 317–325.
Eggins, S., Grün, R., Pike, A.W.G., Shelley, M., Taylor, L., 2003. ^{238}U, ^{232}Th profiling and U-series isotope analysis of fossil teeth by laser ablation-ICPMS. Quat. Sci. Rev. 22, 1373–1382.
Galer, S.J., 1999. Optimal double and triple spiking for high precision lead isotopic measurement. Chem. Geol. 157, 255–274.
Gallup, C.D., Lawrence, R.L., Johnson, R.G., 1994. The timing of high sea levels over the past 200,000 years. Science 263, 796–800.
Harvey, B.G., 1962. Introduction to Nuclear Physics and Chemistry. Prentice Hall Inc, New Jersey. 370 pp.
Henderson, G.M., Slowey, N.C., 2000. Evidence from U–Th dating against Northern Hemisphere forcing of the penultimate glaciation. Nature 404, 61–66.
Hinners, T.A., Hughes, R., Outridge, P.M., Davis, W.J., Simon, K., Woolard, D.R., 1998. Interlaboratory comparison of mass spectrometric methods for lead isotopes and trace elements in NIST SRM 1400 Bone Ash. J. Anal. At. Spectrom. 13, 963–970.
Ikeya, M., 1982. A model of linear uranium uptake for ESR age of Heidelberg (Mauer) and Tautavel bones. Jpn. J. Appl. Phys. (Lett.) 21, 690–692.
Kronfeld, J., Vogel, J.C., 1991. Uranium isotopes in surface waters from southern Africa. Earth Planet. Sci. Lett. 105, 191–195.
Kronfeld, J., Vogel, J.C., Talma, A.S., 1994. A new explanation for extreme ^{234}U/^{238}U disequilibria in a dolomitic aquifer. Earth Planet. Sci. Lett. 123, 81–93.
Leakey, M.D., 1970. Stone artefacts from Swartkrans. Nature 225, 1222–1225.
Millard, A.R., Hedges, R.E.M., 1996. A diffusion–adsorption model of uranium uptake by archaeological bone. Geochim. Cosmochim. Acta 60, 2139–2152.
Morse, J.W., Shanbhag, P.M., Saito, A., Choppin, G.R., 1984. Interaction of uranyl ions in carbonate media. Chem. Geol. 42, 85–99.
Partridge, T.C., Shaw, J., Heslop, D., Clarke, R.J., 1999. The new hominid skeleton from Sterkfontein, South Africa: age and preliminary assessment. J. Quat. Sci. 14, 293–298.
Partridge, T.C., Granger, D.E., Caffee, M.W., Clarke, R.J., 2003. Lower Pliocene hominid remains from Sterkfontein. Science 300, 607–612.
Pike, A.W.G., Hedges, R.E.M., Van Calsteren, P., 2002. U-series dating of bone using the diffusion–adsorption model. Geochim. Cosmochim. Acta 66, 4273–4286.
Reynard, B., Lecuyer, C., Grandjean, P., 1999. Crystal-chemical controls on rare-earth element concentrations in fossil biogenic apatites and implications for paleoenvironmental reconstructions. Chem. Geol. 155, 233–241.
Robinson, J.T., 1953. The nature of Telanthropus capensis. Nature 171, 33.
Robinson, J.T., 1970. New finds at the Swartkrans Australopithecines Site (contd). Nature 225, 1217–1219.
Stacey, J.S., Kramers, J.D., 1975. Approximation of terrestrial lead isotope evolution by a two-stage model. Earth Planet. Sci. Lett. 26, 207–221.
Susman, R.L., de Ruiter, D., Brain, C.K., 2001. Recently identified postcranial remains of Paranthropus and Early Homo from Swartkrans Cave, South Africa. J. Hum. Evol. 41, 607–629.
Thackeray, J.F., Kirschvink, J.L., Raub, T.D., 2002. Palaeomagnetic analyses of calcified deposits from the Plio–Pleistocene hominid site of Kromdraai, South Africa. S. Afr. J. Sci. 98, 1–4.
Thompson, W.G., Spiegelman, M.W., Goldstein, S.L., Speed, R.C., 2003. An open-system model for U-series age determinations of fossil corals. Earth Planet. Sci. Lett. 210, 365–381.
Villemant, B., Feuillet, N., 2003. Dating open systems by the ^{238}U–^{234}U–^{230}Th method: application to Quaternary reef terraces. Earth Planet. Sci. Lett. 210, 105–118.
Vrba, E.S., 1975. Some evidence of chronology and palaeoecology of Sterkfontein, Swartkrans and Kromdraai from the fossil Bovidae. Nature 254, 301–304.
Vrba, E.S., 1985. Early hominids in southern Africa: updated observations on chronological and ecological background. In: Tobias, P.V. (Ed.), Hominid Evolution: Past, Present and Future. Alan R. Liss, New York, pp. 195–200.
Walker, J., Cliff, R.A., Latham, A.G., 2006. U–Pb Isotopic Age of the StW 573 Hominid from Sterkfontein, South Africa. Science 314, 1592–1594.
White, T.D., 1988. The comparative biology of "robust" *Australopithecus*: clues from context. In: Grine, F.E. (Ed.), Evolutionary History of the 'Robust' Australopithecines. Aldine de Gruyter, New York, pp. 449–483.
White, W.M., Albarède, F., Télouk, P., 2000. High-precision analysis of Pb isotopic ratios using multi-collector ICP-MS. Chem. Geol. 167, 257–270.
Woodhead, J., Hellstrom, J., Maas, R., Drysdale, R., Zanchetta, G., Devine, P., Taylor, E., 2006. U–Pb geochronology of speleothems by MC-ICPMS. Quat. Geochron. 1, 208–221.